Analytical Methods

ROYAL SOCIETY OF CHEMISTRY

PAPER

View Article Online
View Journal | View Issue

Cite this: *Anal. Methods*, 2026, **18**, 2225

Expanding luminol activity: UV-enhanced peroxidase-like activity for dual-mode wide-pH biosensing

Mohamed Hassan Mahana,[a] Syed Rahin Ahmed,[b] Poushali Das,[a] Seshasai Srinivasan *[ab] and Amin Reza Rajabzadeh *[ab]

While luminol is typically employed for its chemiluminescence in basic media, this report uncovers a previously unrecognized function: a strong peroxidase-like activity in acidic environments, enabling a colorimetric sensing modality that complements its well-established chemiluminescence under basic conditions. By integrating these dual functionalities, luminol can serve as a broad-pH, dual-mode sensing reagent, laying the groundwork for microfluidic systems that provide colorimetric detection when the sample is acidic and chemiluminescent detection when the sample is basic. Specifically, the peroxidase-like activity of luminol was leveraged in this study to establish a colorimetric assay for the detection of H_2O_2 and dopamine. Under optimized conditions, the proposed detection method enabled reliable monitoring of H_2O_2 and dopamine with limit of detection (LOD) values of 0.0149 mM and 0.52 μM, respectively. This study also reveals that UV activation substantially enhances luminol's peroxidase-like activity, decreasing the detection time from 35 to 4.5 min and improving the sensitivity by lowering the LOD from 0.0149 to 0.0085 mM. Kinetic studies using Michaelis–Menten and Lineweaver–Burk analyses demonstrate that luminol exhibits high peroxidase-like catalytic competency compared with other reported nanozymes. Moreover, the method was successfully applied for the determination of dopamine in a simulated blood sample, achieving an LOD value of 1.5089 μM, thereby demonstrating its excellent performance and suitability for dopamine analysis in complex biological environments. These findings highlight the use of luminol as an efficient, UV-enhanced peroxidase mimic with strong potential as a rapid and sensitive platform for next-generation colorimetric biosensors in clinical applications.

Received 19th December 2025
Accepted 9th February 2026

DOI: 10.1039/d5ay02106e

rsc.li/methods

1. Introduction

Luminol is a chemical substance that exhibits blue luminescence upon reaction with specific oxidizing agents.[1] It is one of the most widely employed chemiluminescent reagents in forensic science and biochemical assays due to its accessibility and cost-effectiveness.[1] Chemiluminescence is the emission of electromagnetic radiation resulting from a chemical reaction.[2] Luminol has been extensively applied in several analytical contexts, including trace metal analysis, immunoassays, free radical detection, environmental monitoring, and forensic investigations.[3–7] It is widely used in forensic science because it helps identify the presence of blood at crime scenes.[3] The chemiluminescent signal arises when the basic solution of luminol is oxidized by an oxidizing agent such as hydrogen peroxide (H_2O_2) in the presence of catalyzing agents.[8,9] In forensic applications, the luminol solution is typically combined with H_2O_2 and applied to surfaces suspected of blood contamination. The iron-rich protein hemoglobin in blood contains heme, which acts as the catalyzing agent for the chemiluminescent reaction, facilitating the oxidation of luminol and resulting in the emission of visible light if blood is present.[8]

Enzyme-like activity of various nanomaterials (nanozymes) has recently attracted significant research interest owing to their stability under harsh conditions, low toxicity, excellent catalytic activity, affordability, increased selectivity and ease of surface modification.[10,11] Nanozymes are regarded as promising alternatives to natural enzymes, which are often less stable, more expensive to obtain, and challenging to store.[12] Nanozymes have been widely employed in several applications such as biosensors, drug delivery, bioimaging, environmental analysis, and antibacterial therapies.[13–19]

In peroxidase reactions, hydroxyl radicals generated from the decomposition of H_2O_2 initiate the oxidation of peroxidase substrates such as TMB to oxidized TMB and generate a blue color for colorimetric detection.[12] Most of the reported

[a]*School of Biomedical Engineering, McMaster University, 1280 Main Street West, Hamilton, Ontario, Canada. E-mail: ssriniv@mcmaster.ca; rajaba@mcmaster.ca*
[b]*School of Engineering Practice and Technology, McMaster University, 1280 Main Street West, Hamilton, Ontario, Canada*

peroxidase reactions occur only in an acidic environment where H_2O_2 serves as an electron donor and undergoes decomposition on the surface of the nanozyme, thereby enhancing the production of hydroxyl radicals.[20] On the other hand, the luminol-based chemiluminescent reaction occurs when luminol reacts with H_2O_2 in a basic medium in the presence of a suitable catalyst such as iron salt. The chemiluminescent mechanism begins with the deprotonation of luminol to form a dianion, which subsequently reacts with H_2O_2 in the presence of the catalyst to generate 3-aminophthalate in an electronically excited state, which then relaxes to the ground state, emitting chemiluminescent light at 425 nm.[21] Luminol is protonated in an acidic environment, which inhibits the chemiluminescent reaction, so the reaction occurs only in a basic environment. By exploring the peroxidase-like reaction of luminol in an acidic environment, the proposed platform can be considered as a tool to develop an integrated microfluidic device that can be used for the detection of H_2O_2 in both pH environments. The microfluidic device is composed of two channels, one channel for the peroxidase reaction, which contains luminol and TMB, while the second channel for the chemiluminescent reaction, which contains luminol and a catalyst like iron salt (Fig. 1). A single H_2O_2-containing sample can be split into two reaction channels to provide either a colorimetric signal at 660 nm in the peroxidase channel if the sample is acidic or a chemiluminescent signal at 425 nm in the chemiluminescent channel if the sample is basic. Consequently, this integrated microfluidic system not only facilitates H_2O_2 detection under varying pH conditions but also provides information regarding the sample's acidity or alkalinity.

Dopamine is a chemical messenger that works in several parts of the human brain and gives sensations of happiness, satisfaction, and motivation. It also has an important effect in the regulation of sleep cycles, mood, attention, movement, and memory.[22] Dopamine dysregulation is a key feature of numerous neurological and psychiatric disorders. Reduced dopamine levels are associated with Parkinson's disease, schizophrenia, and depression, whereas elevated dopamine levels have been linked to hallucinations, anxiety, and sleep disturbances.[23,24] Therefore, accurate and continuous monitoring of dopamine concentrations is vital for the diagnosis and management of these neurological and psychiatric disorders. Traditional detection methods largely rely on biomolecules such as enzymes or antibodies, which pose challenges due to their high production costs and vulnerability to temperature fluctuations.[25,26] Chemicals with enzyme-mimicking characteristics can be utilized to overcome many problems associated with biomolecules. H_2O_2 is another vital biological substance that plays essential roles in oxidative biosynthetic processes, cellular signaling, metabolism, host defense and oxidative stress.[27,28] Variations in H_2O_2 levels can reflect metabolic abnormalities associated with lung diseases, diabetes and other

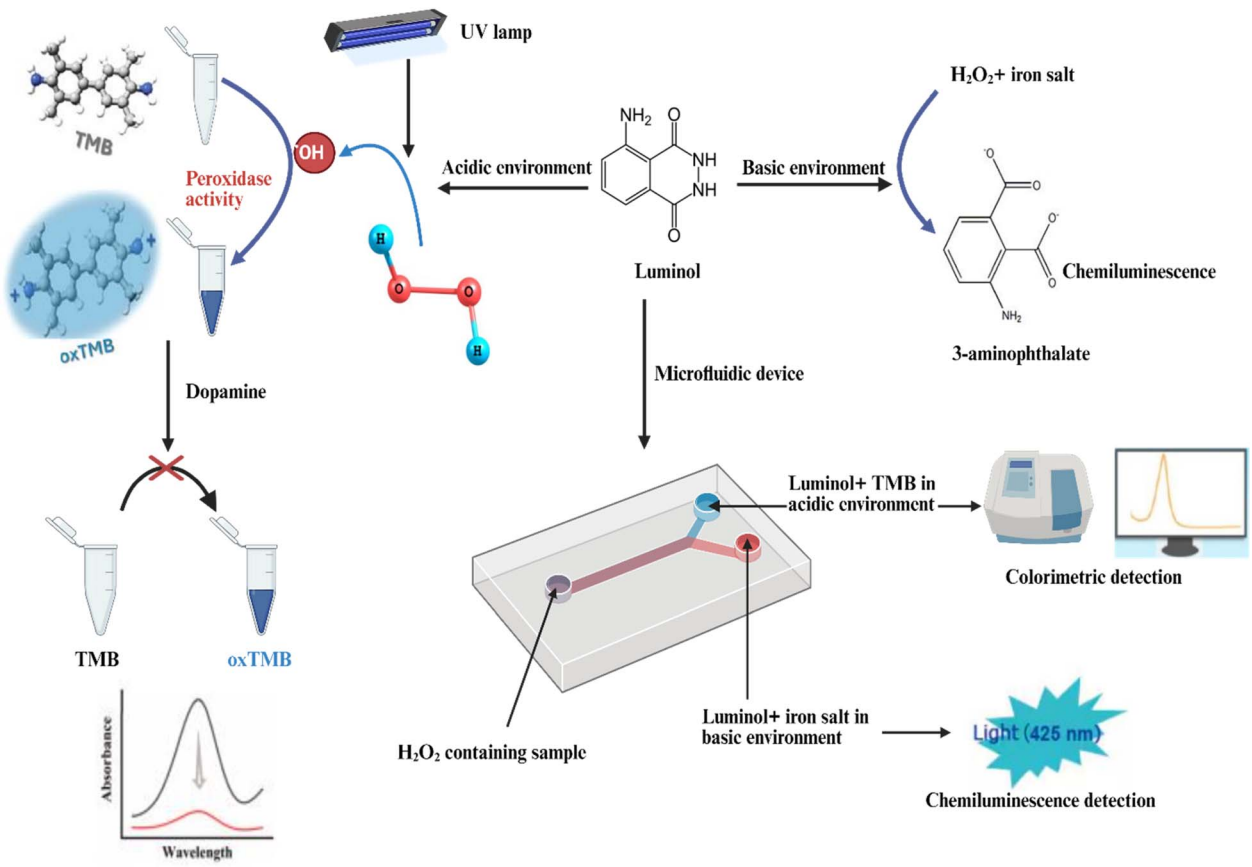

Fig. 1 The integrated microfluidic device.

health issues.[29] The concentrations of H_2O_2 that exceed certain thresholds are regarded as hazardous to human health, particularly when inhaled or ingested,[30] underscoring the importance of monitoring its concentration to ensure it remains within a safe physiological range.

This study presents the peroxidase-like activity of luminol to develop a colorimetric assay for the detection of H_2O_2 and dopamine. Exposure of luminol to UV light (395 nm) significantly enhanced its peroxidase-like activity, leading to a marked reduction in detection time and improved analytical sensitivity, as evidenced by a lower limit of detection (LOD). The dopamine detection assay relied on dopamine's ability to inhibit the peroxidase-like activity of luminol, enabling quantification based on the corresponding decrease in the blue color. Moreover, a selectivity study was carried out, and it proved the high selectivity of the developed method toward dopamine detection in the presence of interfering analytes. Furthermore, the kinetic parameters of luminol were studied, which demonstrated the high competency of peroxidase-like enzyme activity of luminol, compared with some reported nanozymes.

2. Experimental details

2.1 Reagents and materials

Luminol powder, sodium acetate buffer (pH: 5.2 ± 0.1), 3,3′,5,5′-tetramethylbenzidine (TMB) (≥99%), terephthalic acid (98%), glucose (≥99.5%), dimethyl sulfoxide (DMSO) (≥99.9%), L-glutamine (99–101%), sodium carbonate, ascorbic acid (≥99%), uric acid (≥99%), dopamine hydrochloride, 30% w/w hydrogen peroxide (H_2O_2), sucrose (≥99.5%), and potassium hexacyanoferrate were obtained from Sigma-Aldrich (MO, USA). Fructose was bought from VWR Chemicals (Ohio, USA). The simulated blood sample was purchased from Biochemazone (Alberta, Canada).

2.2 Instrumentation

The UV-visible and luminescence measurements were recorded using a BioTek Synergy H1 microplate reader. The Fourier transform infrared (FTIR) spectrum was recorded using a VERTEX 70v FTIR spectrometer. An analytical balance (VWR, USA), a vortex mixer (Mandel, Taiwan) and an ultrasonic cleaner (Limplus, China) were used.

2.3 Peroxidase-like activity of luminol

A colorimetric detection technique using a UV-visible spectrophotometer was used to evaluate the peroxidase-like activity of luminol. In a 96-well microplate, 20 μl of TMB solution, with a concentration of 10 mM, was mixed with 100 μl of H_2O_2 solution (10 mM). Then, 200 μl of luminol solution (1 mg ml^{-1}) was added, and the mixture was left to react for 35 min at room temperature. After the specified time, the absorption spectrum of the reaction product was recorded, and a blue color formed.

2.4 H_2O_2 detection

2.4.1 Preparation of H_2O_2 standard and working solutions. A standard solution of H_2O_2, with a concentration of 20 mM, was prepared by transferring 52 μl of 30% w/w H_2O_2 stock solution into a Falcon tube, and the volume was adjusted to 25 ml using sodium acetate buffer. Subsequently, another standard H_2O_2 solution, with a concentration of 10 mM was prepared by transferring 5 ml of the above standard solution into another Falcon tube, and the volume was adjusted to 10 ml using sodium acetate buffer. The standard solutions were kept in the refrigerator for further use.

Different volumes from the two standard solutions were transferred into a series of microtubes, and the volume was adjusted to 1 ml in each microtube with sodium acetate buffer to obtain H_2O_2 working solutions with a concentration range of 0–14 mM.

2.4.2 Construction of the H_2O_2 calibration curve. H_2O_2 was determined *via* colorimetric detection measurements through the peroxidase-like activity of luminol. In a 96-well microplate, aliquots of 20 μl of TMB solution (16 mM) were mixed with aliquots of 100 μl of different H_2O_2 concentrations (0–14 mM), followed by the addition of aliquots of 200 μl of luminol solution (1 mg ml^{-1}). The mixtures were allowed to react for 35 minutes at room temperature. After the specified time, the absorbance value of each concentration was measured at 660 nm. The control experiment was carried out concurrently. To get the calibration curve, the absorbance values at 660 nm were plotted *versus* the corresponding H_2O_2 concentrations.

2.4.3 UV-assisted peroxidase-like activity of luminol. A second method for H_2O_2 detection was performed using the peroxidase-like activity of luminol with the assistance of UV light. In a 96-well microplate, aliquots of 20 μl of TMB solution (10 mM) were mixed with aliquots of 100 μl of different H_2O_2 concentrations (0–14 mM), followed by the addition of aliquots of 200 μl of luminol solution (1 mg ml^{-1}). The reaction mixtures were then exposed to a UV lamp (395 nm) for 4.5 minutes at room temperature. After the specified time, the absorbance value of each concentration was measured at 660 nm, and the absorbance values were plotted *versus* the corresponding H_2O_2 concentrations.

2.5 Dopamine detection

The detection method of dopamine is based on the suppression of the blue color of the peroxidase-like activity of luminol. In 96-well microplate, aliquots of 100 μl of H_2O_2 solution (16 mM) were mixed with aliquots of 20 μl of TMB solution (18 mM), followed by the addition of aliquots of 120 μl of luminol solution (1.5 mg ml^{-1}) and 100 μl of different dopamine aqueous solutions (5–1000 μM). The mixtures were allowed to react for 35 minutes at room temperature. After the specified time, the absorbance value of each concentration was measured at 660 nm. The control experiment was conducted simultaneously. To get the calibration curve, the absorbance ratios (A^0/A) at 660 nm were plotted *versus* the corresponding dopamine concentrations. A^0 represents the absorbance measured at 660 nm when dopamine was absent (control experiment) and A denotes the absorbance measured at 660 nm in the presence of dopamine concentrations (5–1000 μM), and the regression data were obtained. To detect dopamine in blood, simulated blood

samples were spiked with dopamine to get dopamine solutions with the concentrations of 5–1000 μM, and the peroxidase reaction of luminol was carried out as mentioned above. The calibration curve was obtained by plotting the absorbance ratios (A^0/A) at 660 nm *versus* the corresponding dopamine concentrations.

2.6 Selectivity testing

To assess the selectivity of the proposed colorimetric assay for dopamine detection, various potentially interfering substances were examined, including uric acid, ascorbic acid, fructose, glutamine, sucrose, glucose, epinephrine, and serotonin. Stock aqueous solutions of each interfering substances were prepared with a concentration of 1 mg ml^{-1}. Then, different aliquots of each interfering substance solution were taken and diluted with deionized water to get interfering substance solutions with the concentrations of 1 mM. In a 96-well plate, aliquots of 100 μl of H_2O_2 solution (16 mM) were mixed with aliquots of 20 μl of TMB solution (18 mM), followed by addition of aliquots of 120 μl of luminol solution (1.5 mg ml^{-1}) and 100 μl of each interfering substance solution (1 mM). The mixtures were allowed to react for 35 minutes at room temperature. Subsequently, the absorbance value of each well was measured at 660 nm. The control experiment and dopamine determination were conducted concurrently.

2.7 Terephthalic acid (TA) testing

The terephthalic acid (TA) test was performed to prove the generation of hydroxyl radicals. First, 50 μl of TA solution (2 mM) was mixed with 150 μl of luminol solution (1 mg ml^{-1}) and was left for 10 minutes. After that, 150 μl of H_2O_2 solution (10 mM) was added to the mixture and was allowed to react at room temperature for 30 minutes. Then, a spectrofluorometer was used to record the fluorescence emission spectrum of the reaction product.

2.8 Kinetic studies of peroxidase-like activity of luminol

The kinetic parameters of peroxidase-like activity of luminol were evaluated by measuring the absorbance at 660 nm using varying TMB and H_2O_2 concentrations. Using TMB as the substrate, the absorbance values were measured at 660 nm using different TMB concentrations (0–20 mM) and keeping the H_2O_2 concentration constant at 10 mM. For H_2O_2 as the substrate, the absorbance values were measured at 660 nm using the H_2O_2 concentration range of 0–20 mM, while the TMB concentration was kept constant at 10 mM.

3. Results and discussion

3.1 Characterization of luminol

The UV-visible absorption spectrum of luminol is presented in Fig. 2a, which reveals three characteristic absorbance peaks of luminol located at 221 nm, 300 nm and 347 nm. The two peaks at 221 nm and 300 nm correspond to π–π* electronic transitions, and the third one at 347 nm is due to n–π* electronic transitions.[31,32] The chemiluminescence spectrum of luminol was also recorded by mixing the basic solution of luminol with H_2O_2 in the presence of potassium hexacyanoferrate (iron salt) as a catalyst. Fig. 2b shows the characteristic emission peak of luminol at 425 nm.[1] The FTIR spectrum of luminol was recorded, and it shows the characteristic peaks of N–H stretching vibration at 3410 cm^{-1} and C=O stretching vibration at 1657 cm^{-1}. The two peaks at 1495 cm^{-1} and 1316 cm^{-1} correspond to the vibrations from C=C and C–N, respectively[33] (Fig. 2c).

3.2 Peroxidase-like activity of luminol

The colorimetric detection technique is one of the most popular detection methods because of its many advantages, which include its sensitivity, affordability, wide availability, and ease of use.[34] Free radicals start the oxidation reaction of peroxidase substrates that leads to the formation of colored products with signals for colorimetric detection of target analytes. For example, in the reaction between H_2O_2 and TMB, the hydroxyl free radicals are generated from the decomposition of H_2O_2, which causes the oxidation of TMB, changing it into oxidized TMB and generating a blue color.[35]

To investigate the peroxidase mimic activity of luminol, the UV-vis spectra of several H_2O_2, TMB, and luminol combinations were collected. As demonstrated in Fig. 2d, only the solution that contained H_2O_2, TMB and luminol showed a deep blue color with a high absorbance peak at 660 nm (λ_{max} of oxidized TMB), while other combinations did not change. These results confirmed that TMB was oxidized in the presence of luminol and H_2O_2 due to the peroxidase-like activity of luminol.

3.3 Detection of H_2O_2

3.3.1 Optimization of H_2O_2 detection parameters. Different factors affecting the detection of H_2O_2 were investigated and optimized to get the best peroxidase-like activity of luminol. The aim was to enhance the sensitivity of the suggested method by improving the product yield.

3.3.1.1 Optimization of luminol concentration. The effect of luminol concentration was studied by determining the concentration of luminol that produced the highest absorbance at 660 nm with the deepest blue color. Several luminol concentrations were evaluated (0.125–2 mg ml^{-1}), and the blank experiment was carried out concurrently. The peroxidase-like activity test was performed for each luminol concentration as mentioned before (Section 2.3). The absorbance value at 660 nm was recorded for each luminol concentration, while the concentrations of TMB and H_2O_2 were kept fixed at 10 mM. The results demonstrated that the optimum concentration of luminol was 1 mg ml^{-1} (Fig. S1).

3.3.1.2 Optimization of TMB concentration. Different TMB concentrations were prepared (2–20 mM), and the peroxidase-like activity test was carried out for each TMB concentration as mentioned before. The blank experiment was conducted concurrently. The absorbance value at 660 nm was recorded for each TMB concentration, while the concentrations of luminol and H_2O_2 were fixed at 1 mg ml^{-1} and 10 mM, respectively. The absorbance value increased upon increasing the concentration

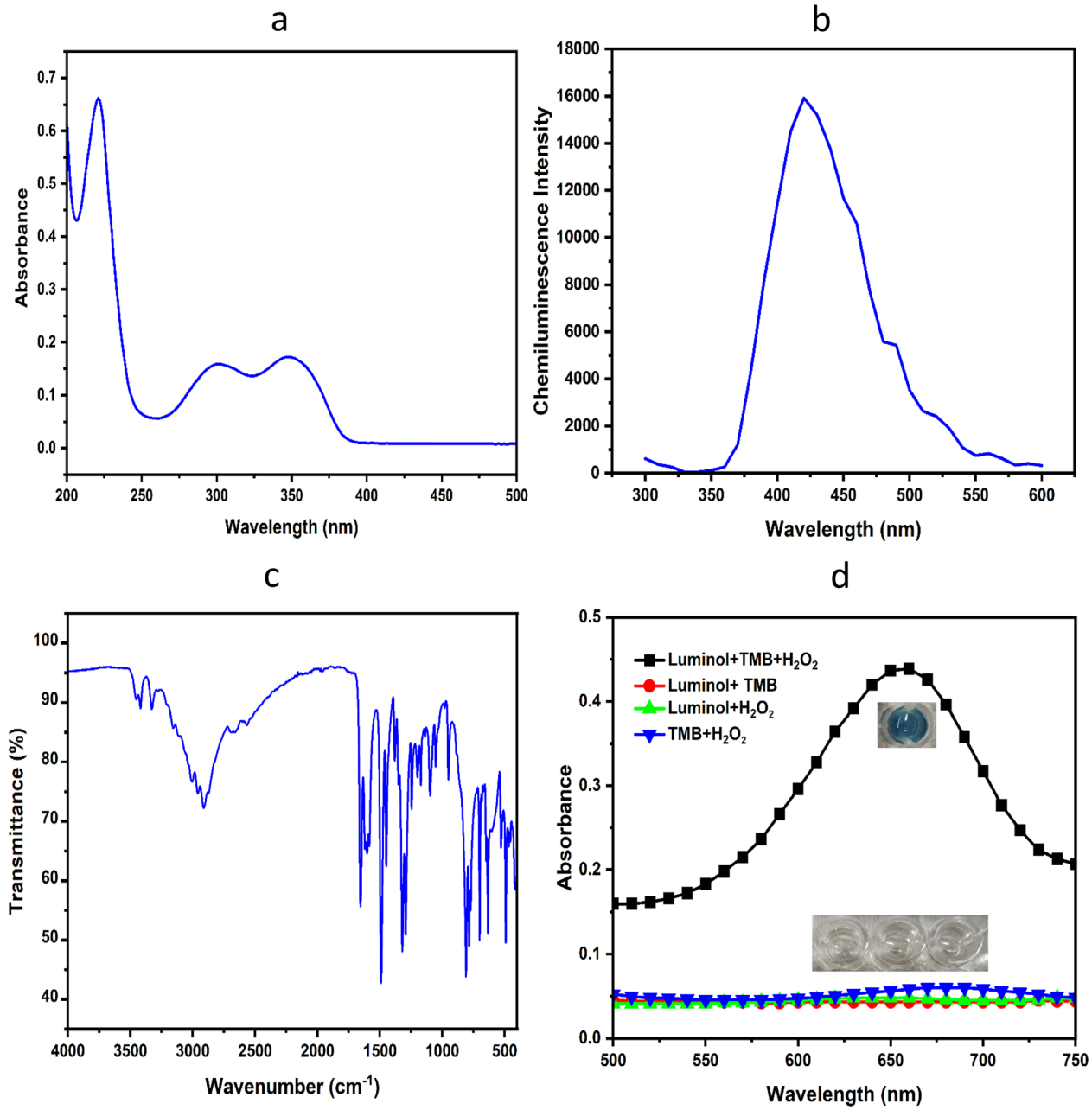

Fig. 2 (a) UV-visible spectrum of luminol, (b) chemiluminescence spectrum of luminol (it was recorded by mixing the basic solution of luminol with H_2O_2 in the presence of potassium hexacyanoferrate as a catalyst), (c) FTIR spectrum of luminol, (d) peroxidase-like activity of luminol (it was evaluated by recording the absorption spectra of the reaction products of different combinations of H_2O_2 (10 mM), TMB (10 mM) and luminol (1 mg ml^{-1}) after 35 min at room temperature).

of TMB, before plateauing at a TMB concentration of 16 mM (Fig. S2). So, 16 mM TMB was used for further experiments.

3.3.1.3 Buffer optimization. Two buffers were investigated with different pH values, phosphate buffered saline (PBS) (pH 7.4) and sodium acetate buffer (SAB) (pH: 5.2). The concentrations of luminol, TMB and H_2O_2 were fixed at 1 mg ml^{-1}, 16 mM and 10 mM, respectively. The results demonstrated that the more acidic environment of SAB resulted in a higher absorbance value at 660 nm with a deeper blue color than PBS (Fig. S3).

3.3.1.4 Optimization of the reaction time. The effect of reaction time was also optimized by measuring the absorbance values at 660 nm every 5 minutes. As shown in Fig. S4, the deepest blue color with the highest absorbance value at 660 nm was recorded after 35 minutes before reaching a plateau. Therefore, the optimum reaction time was 35 minutes.

3.3.2 Determination of H_2O_2. The mean absorbance values at 660 nm were plotted *versus* the corresponding H_2O_2 concentrations to get the calibration curve. As shown in Fig. 3, the linearity of the proposed method was found to be at H_2O_2

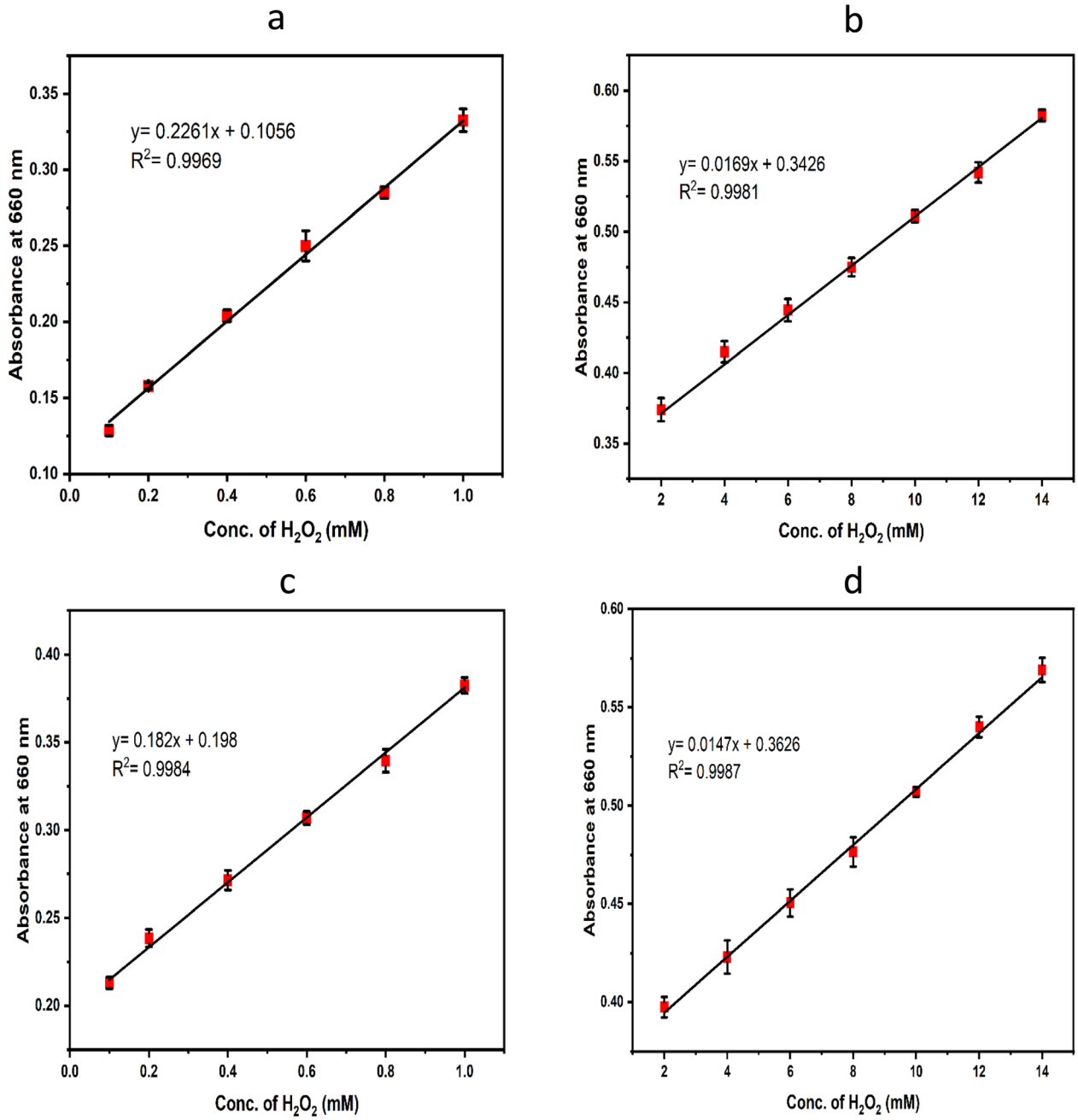

Fig. 3 Calibration curves of H_2O_2 using the proposed method (different H_2O_2 concentrations were mixed with TMB (16 mM) and luminol (1 mg ml^{-1}) and the absorbance values were measured at 660 nm after 35 min): (a) (0.1–1 mM) and (b) (2–14 mM). Calibration curves of H_2O_2 using the UV-assisted method (different H_2O_2 concentrations were mixed with TMB (16 mM) and luminol (1 mg ml^{-1}), the reaction mixtures were then exposed to a UV lamp (395 nm) for 4.5 min, and the absorbance values were measured at 660 nm): (c) (0.1–1 mM) and (d) (2–14 mM).

concentrations of 0.1–14 mM. The suggested method's good linearity was indicated by the high coefficient of determination value of the calibration curve ($r^2 = 0.9969$) (Table S1). The following equation was used to calculate the detection limit (LOD)

$$\mathrm{LOD} = 3.3 \times \sigma/S \quad (1)$$

where S is the slope of the calibration curve, and σ refers to the standard deviation of the absorbance values for three blank measurements. The low LOD value (0.0149 mM) proved the high sensitivity of the developed method, compared with some reported peroxidase-based H_2O_2 detection methods (Table 1).

The second method for H_2O_2 detection was carried out with the assistance of UV light to enhance the peroxidase-like activity of luminol (Fig. 4). The detection time decreased from 35 min in the conventional method to 4.5 min in the UV-assisted method. The proposed method was found to be linear over the concentration range of 0.1–14 mM (Fig. 3), with a coefficient of determination value of $R^2 = 0.9984$, indicating the excellent linearity

Table 1 Comparison of the LOD of the suggested method with some reported peroxidase-based H_2O_2 detection methods

Material	LOD (mM)	Method	Linearity range (mM)	Ref.
Au–Ag–Pt NPs	0.054	Colorimetry	0.05–1	39
Ni–MOF nanosheets	0.04	Fluorescence	0.1–20	40
Au@PNIPAm	2.43	Colorimetry	3–15	41
VO_2 nanosheets	0.266	Colorimetry	0.488–62.5	42
Pd–Pt–Ir	3.6	Colorimetry	3.9–62.5	43
Luminol	0.0149	Colorimetry	0.1–14	This work
UV-assisted luminol	0.0085	Colorimetry	0.1–14	This work

of the proposed method. The LOD was calculated using eqn (1), and it was found to be 0.0085 mM. The calculated LOD for the UV-assisted method was 1.7-fold lower than the conventional method. So, by employing UV light for the reaction, the peroxidase-like activity of luminol was enhanced, and the detection time was extensively decreased. Also, the LOD of the proposed method was decreased, which enables the detection of lower concentrations of H_2O_2 and enhances the sensitivity of the proposed method. The enhancement of peroxidase-like activity of luminol may be due to the effect of UV light on H_2O_2. UV light facilitates the decomposition of H_2O_2 according to the following reaction:[36]

$$H_2O_2 + h\nu \rightarrow 2OH^{\cdot}$$

In H_2O_2, the relative strength of the O–O bond is of vital importance from a mechanistic perspective. The O–O bond of H_2O_2 is the weakest bond, and it has a bond dissociation energy of about 45 kcal mol^{-1}.[37] When H_2O_2 was irradiated with UV light, the energy of UV photons is sufficient to overcome the bond dissociation energy of the O–O bond resulting in homolytic cleavage of the O–O bond,[38] generating hydroxyl radicals that initiate the peroxidase reaction and cause the oxidation of TMB.

3.4 Dopamine detection

The proposed method was used for colorimetric determination of dopamine. The detection method of dopamine was based on the decrease in the intensity of the blue color of oxidized TMB and the corresponding reduction in absorbance values at 660 nm. An increase in the dopamine concentration was observed to correspond with a decrease in absorbance at 660 nm. This is because dopamine captures hydroxyl radicals,

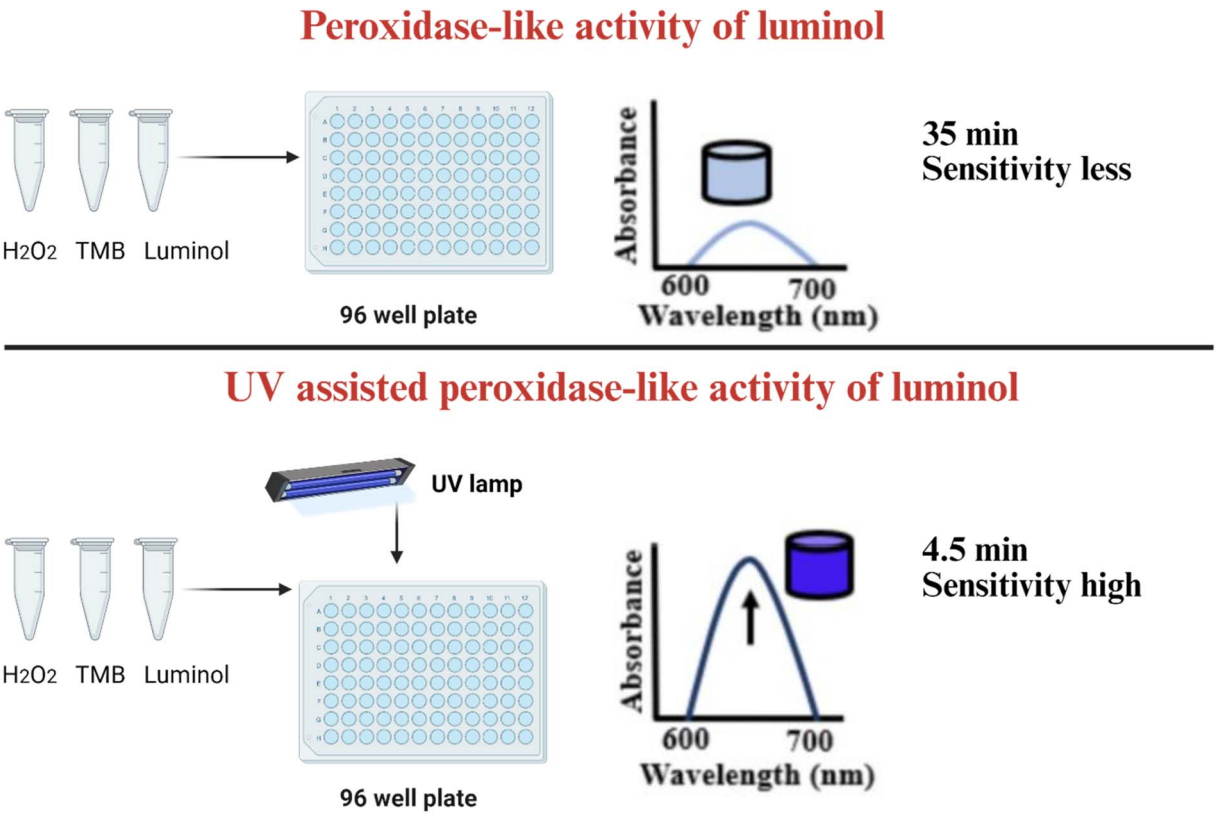

Fig. 4 Schematic presentation of the proposed sensing method.

resulting in a decreased availability of the radicals for the oxidation of TMB.[12,35]

3.4.1 Optimization of dopamine detection parameters

3.4.1.1 Optimization of luminol concentration. The effect of luminol concentration was investigated by determining the concentration of luminol that gave the maximum difference in absorbance at 660 nm in the presence and absence of dopamine. Different luminol concentrations were studied (0.25–2 mg ml^{-1}), and the peroxidase-like activity test was performed for each luminol concentration as mentioned before. The absorbance value at 660 nm was recorded for each luminol concentration in the absence and presence of dopamine, while the concentrations of TMB, H_2O_2 and dopamine were kept fixed at 16 mM, 16 mM, and 400 μM, respectively. The results revealed that a luminol concentration of 1.5 mg ml^{-1} was optimal, as it produced the maximum difference in absorbance at 660 nm in the presence and absence of dopamine (Fig. S5).

3.4.1.2 Optimization of TMB concentration. Various concentrations of TMB ranging from 2 to 20 mM were prepared, and the peroxidase-mimicking activity test was performed for each TMB concentration, as previously described. The absorbance value at 660 nm was recorded for each TMB concentration in the presence and absence of dopamine, while the concentrations of luminol, H_2O_2 and dopamine were fixed at 1.5 mg ml^{-1}, 16 mM and 400 μM, respectively. TMB concentrations of 18 mM and 20 mM produced the maximum difference in absorbance values in the presence and absence of dopamine, as demonstrated in Fig. S6. So, a TMB concentration of 18 mM was selected as the optimum concentration.

3.4.1.3 Optimization of H_2O_2 concentration. Different H_2O_2 concentrations were prepared (2–20 mM), and the peroxidase-like activity test was carried out for each H_2O_2 concentration as mentioned before. The absorbance at 660 nm was measured for each H_2O_2 concentration in the presence and absence of

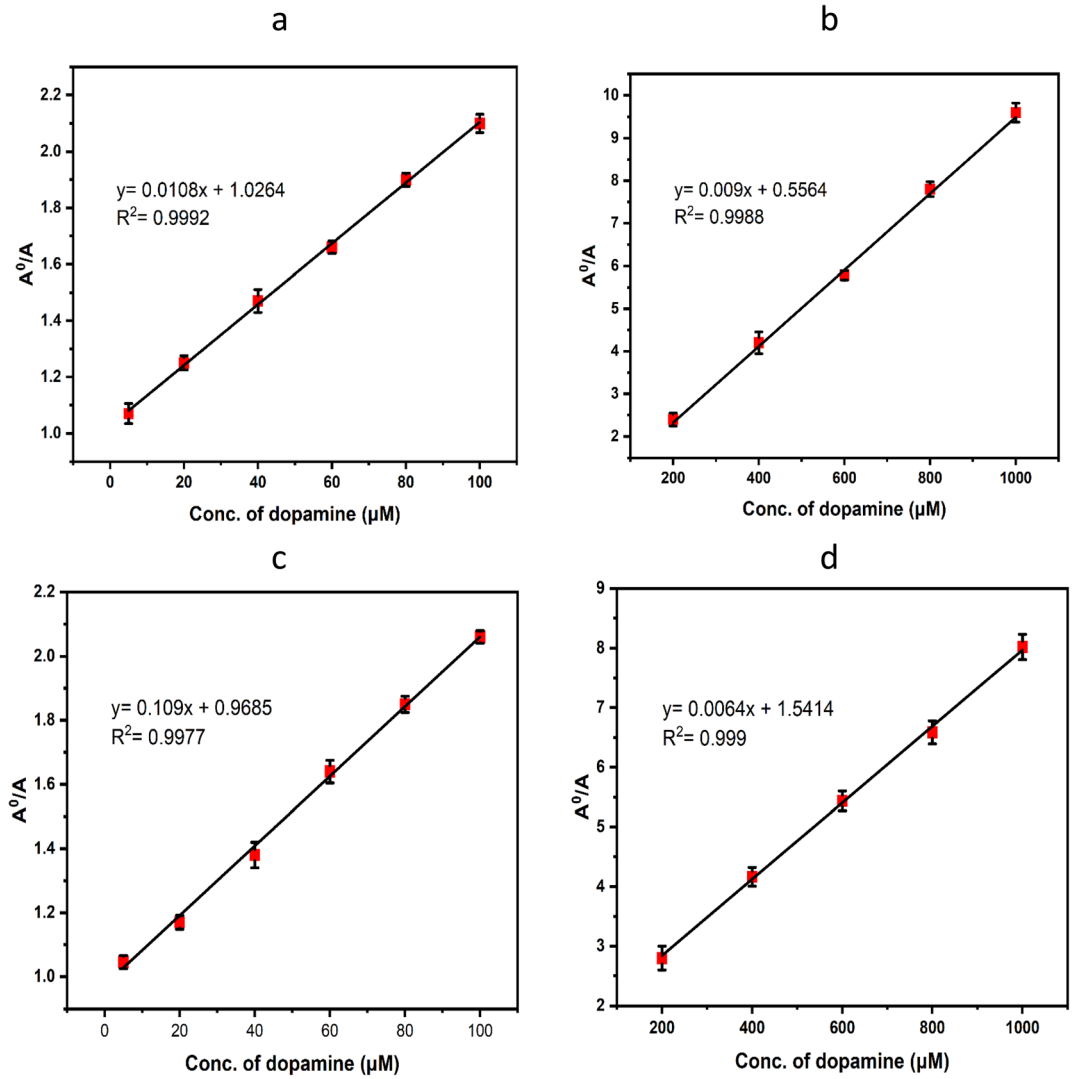

Fig. 5 Calibration curves of dopamine (different dopamine concentrations were mixed with H_2O_2 (16 mM), TMB (18 mM) and luminol (1.5 mg ml^{-1}), and the absorbance values were measured at 660 nm in the presence and absence of dopamine): (a) 5–100 μM and (b) 200–1000 μM. Calibration curves of dopamine in a simulated blood sample (simulated blood samples were spiked with dopamine, and the calibration curves were obtained using the same concentrations of H_2O_2, TMB and luminol): (c) 5–100 μM and (d) 200–1000 μM.

Table 2 Comparison of the LOD of the suggested method with some reported peroxidase-based dopamine detection methods

Nanomaterial	LOD (μM)	Method	Linearity range (μM)	Ref.
AuNPs	2.5	Colorimetry	2.5–20	44
Cu–HMT	4.2	Colorimetry	500–3500	45
MWCNT–FeNAZ–CH	1.05	Electrochemical	7.35–833	46
CQD–AuNP	0.75	Colorimetry	20–80	47
GDY QDs	8.65	Colorimetry	20–100	48
Si QDs	0.5521	Colorimetry	10–1000	12
Luminol	0.52	Colorimetry	5–1000	This work

dopamine, while the concentrations of luminol, TMB, and dopamine were kept constant at 1.5 mg ml^{-1}, 18 mM, and 400 μM, respectively. The increase in the H_2O_2 concentration led to an increase in the absorbance difference at 660 nm between the samples with and without dopamine, reaching a plateau at a concentration of 16 mM (Fig. S7). Therefore, 16 mM H_2O_2 was selected as the optimal concentration for further experiments.

3.4.2 Determination of dopamine. The absorbance ratios (A^0/A) at 660 nm were plotted *versus* the corresponding dopamine concentrations to get the calibration curve. A^0 represents

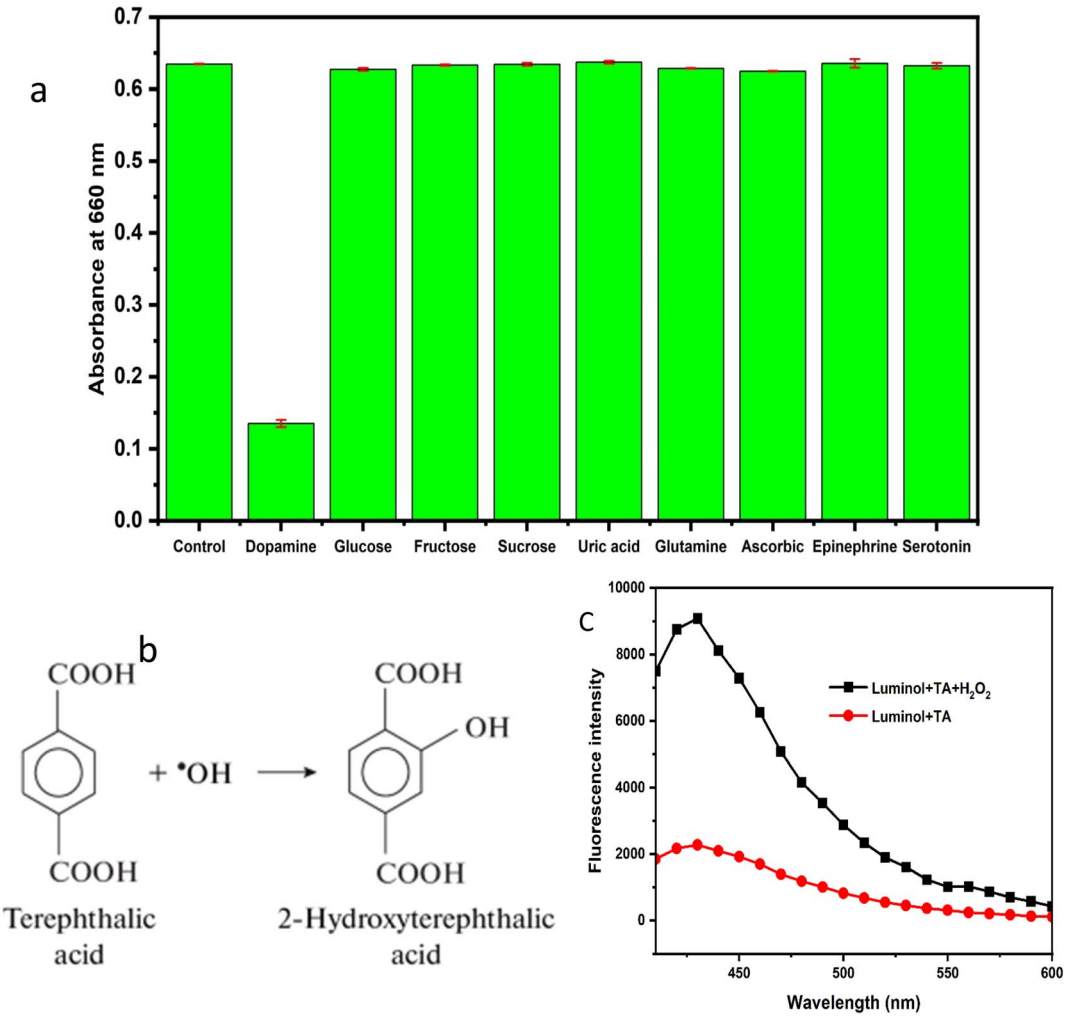

Fig. 6 (a) Selectivity test (interfering substances (1 mM) were mixed with H_2O_2 (16 mM), TMB (18 mM) and luminol (1.5 mg ml^{-1}), and the absorbance values were measured at 660 nm). (b) Reaction of TA with hydroxyl radicals. (c) Fluorescence emission spectrum of the reaction product. (TA solution (2 mM) was mixed with luminol solution (1 mg ml^{-1}) and was left for 10 minutes. After that, H_2O_2 solution (10 mM) was added to the mixture and was allowed to react at room temperature for 30 minutes. Then, a spectrofluorometer was used to record the fluorescence emission spectrum of the reaction product.)

the absorbance measured at 660 nm when dopamine was absent (control experiment), and A denotes the absorbance measured at 660 nm in the presence of dopamine. As shown in Fig. 5, the linearity of the proposed method was found to be over the dopamine concentration range of 5–1000 μM. The suggested method's good linearity was indicated by the high coefficient of determination value of the calibration curve (R^2 = 0.9992) (Table S2). Eqn (1) was used to calculate the LOD. The low LOD value (0.52 mM) confirmed the high sensitivity of the proposed method. A comparison of the LOD achieved in this method with some reported dopamine detection techniques is presented in Table 2, highlighting the superior performance and effectiveness of the developed method. Although the current method demonstrates an improved limit of detection compared to previously reported studies, and considering that normal dopamine levels may be lower than the current LOD, this approach could be suitable for detecting elevated dopamine levels associated with conditions such as hallucinations, anxiety, or sleep disturbances.

3.4.3 Determination of dopamine in a simulated blood matrix. To evaluate the practical applicability of the developed colorimetric method, its performance was tested in a simulated blood matrix, representing a complex biological environment where accurate dopamine detection is critical. This evaluation aimed to test the method's sensitivity, selectivity, and robustness for accurate dopamine detection under conditions mimicking real biological samples. The method demonstrated successful detection of dopamine within the concentration range of 5–1000 μM (Fig. 5). The coefficient of determination (R^2) and LOD were found to be 0.9977 and 1.5089 μM, respectively, confirming the method's excellent linearity and reliability for dopamine determination in complex biological environments such as blood (Table S3).

3.5 Selectivity testing

The selectivity assessment of the developed method was carried out to evaluate the ability of the method to detect dopamine in

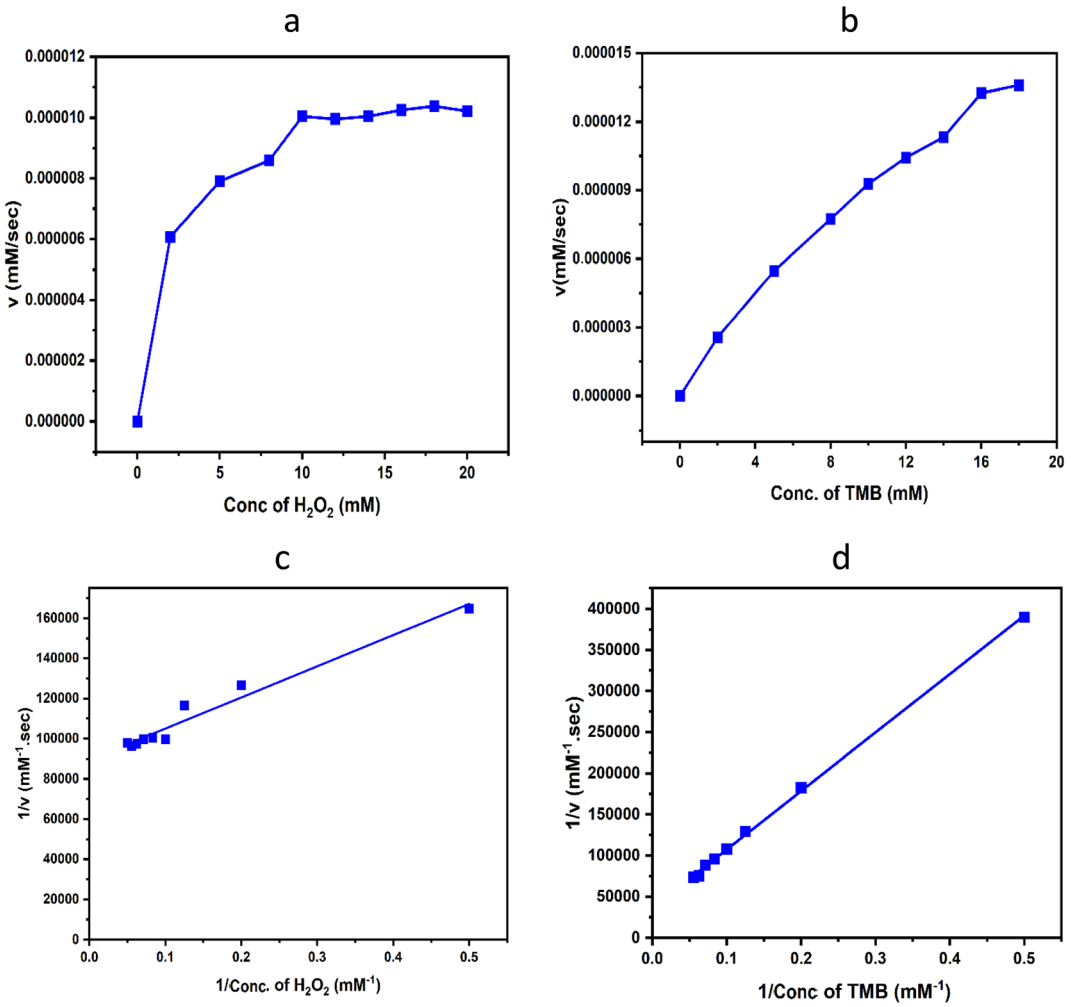

Fig. 7 Kinetic profiles used to calculate the K_m and V_{max}. Michaelis–Menten curves for H_2O_2 (a) and TMB (b). Lineweaver–Burk curves for H_2O_2 (c) and TMB (d). (Using TMB as the substrate, the absorbance values were measured at 660 nm using different TMB concentrations (0–20 mM) and keeping the H_2O_2 concentration constant at 10 mM. For H_2O_2 as the substrate, the absorbance values were measured at 660 nm using the H_2O_2 concentration range of 0–20 mM, while the TMB concentration was kept constant at 10 mM.)

the presence of possible interfering substances. As demonstrated in Fig. 6a, a significant reduction in the intensity of the blue coloration and a marked decrease in absorbance at 660 nm were observed only in the presence of dopamine, while other interfering substances had negligible effects. These results confirm that the method is highly selective for dopamine, demonstrating minimal interference from other coexisting compounds and highlighting its suitability for accurate detection in complex matrices.

3.6 Terephthalic acid (TA) testing

To verify the formation of hydroxyl radicals, a TA test was performed. It is commonly known that hydroxyl radicals cause TA to oxidize, producing the fluorescent product 2-hydroxyterephthalic acid, as shown in Fig. 6b. The solution containing H_2O_2, TA and luminol showed a strong emission fluorescence at 430 nm compared to the solution without H_2O_2 (Fig. 6c), confirming the formation of hydroxyl radicals in the reaction medium.

3.7 Kinetic studies of peroxidase-like activity of luminol

The kinetic studies of peroxidase-like activity of luminol were performed using Michaelis–Menten and Lineweaver–Burk curves (Fig. 7). The concentration of the substrate at which the enzyme reaches half of its maximal velocity (V_{max}) is known as the Michaelis–Menten constant (K_m). The greater the affinity between the substrate and the enzyme, the lower the K_m value.[49] The K_m values were found to be 18.4 mM and 1.7 mM for TMB and H_2O_2, respectively. The kinetic parameters (K_m and V_{max}) were compared with some reported nanozymes, as demonstrated in Tables 3 and 4, showing the high competency of peroxidase-like activity of luminol.

Table 3 Comparison of K_m and V_{max} values of the current study with previously reported data using TMB as the substrate

Nanomaterial	K_m (mM)	V_{max} (mM s^{-1})	Ref.
CoOOH	2	4.74×10^{-5}	50
Nanoceria	3.8	7×10^{-4}	51
CuZnFeS	2.2	3.9×10^{-4}	52
WS_2/rGO	22.4	9.6×10^{-6}	53
MoS_2–$Pt_{74}Ag_{26}$	25.7	7.29×10^{-5}	54
N-GQDs	11.9	3.8×10^{-6}	55
CQD–AuNP	5	5×10^{-7}	47
Luminol	18.4	2.6×10^{-5}	This work

Table 4 Comparison of K_m and V_{max} values of the current study with previously reported data using H_2O_2 as the substrate

Nanomaterial	K_m (mM)	V_{max} (mM s^{-1})	Ref.
$Cu_2(OH)_3Cl$–CeO_2	11.6	8.15×10^{-5}	56
Brominated graphene (GBR)	10.9	3.6×10^{-7}	57
AuNPs	33	6.1×10^{-5}	58
Gold ferritin	199.4	9.34×10^{-5}	59
Fe_3O_4–COOH	65.3	14.02	60
PBMNPs3	323.6	1.17×10^{-3}	61
Fe_3O_4@Pt	702.6	7.13×10^{-4}	62
Fe_3O_4	1175.3	2.40×10^{-4}	62
V_2O_5 NPs	26.47	—	63
Luminol	1.7	1.1×10^{-5}	This work

4. Conclusion

This study demonstrates a strong peroxidase-like activity of luminol in acidic environments, enabling colorimetric detection that complements its chemiluminescence in basic media. This dual functionality, combined with UV enhancement, establishes luminol as a promising agent for the development of versatile broad-pH biosensing platforms. The assay relied on hydroxyl radicals from H_2O_2 decomposition to oxidize TMB to its oxidized form, producing the characteristic blue color in the presence of luminol, which allowed the colorimetric detection of H_2O_2 and dopamine. The kinetic parameters were investigated and compared with some reported peroxidase-based detection methods, proving the high competency of the peroxidase-like activity of luminol. The method was applied for H_2O_2 and dopamine detection with LODs of 0.0149 mM and 0.52 μM, respectively, confirming the high sensitivity of the developed method. UV illumination significantly enhanced luminol's peroxidase-like activity, reducing the detection time from 35 minutes to 4.5 minutes and lowering the LOD to 0.0085 mM. Moreover, the method was successfully employed to detect dopamine in a simulated blood matrix with no interference from the sample matrix. Overall, the current work provides a platform for developing more luminol-based detection systems in future studies.

Conflicts of interest

The authors declare no competing financial interest.

Data availability

The data supporting this article have been included in the paper and as part of the supplementary information (SI). Supplementary information is available. See DOI: https://doi.org/10.1039/d5ay02106e.

Acknowledgements

The authors would like to acknowledge the support from the Natural Sciences and Engineering Research Council of Canada in the form of Discovery Grants to ARR and SS (RGPIN-2019-07246 and RGPIN-2022-04988).

References

1 P. Khan, D. Idrees, M. A. Moxley, J. A. Corbett, F. Ahmad, G. von Figura, W. S. Sly, A. Waheed and M. I. Hassan, Luminol-based chemiluminescent signals: clinical and non-clinical application and future uses, *Appl. Biochem. Biotechnol.*, 2014, **173**, 333–355.

2 M. Liu, Z. Lin and J.-M. Lin, A review on applications of chemiluminescence detection in food analysis, *Anal. Chim. Acta*, 2010, **670**, 1–10.
3 B. A. Stoica, S. Bunescu, A. Neamtu, D. Bulgaru-Iliescu, L. Foia and E. G. Botnariu, Improving luminol blood detection in forensics, *J. Forensic Sci.*, 2016, **61**, 1331–1336.
4 Z. Zhang, J. Lai, K. Wu, X. Huang, S. Guo, L. Zhang and J. Liu, Peroxidase-catalyzed chemiluminescence system and its application in immunoassay, *Talanta*, 2018, **180**, 260–270.
5 S. Deepa, R. Venkatesan, S. Jayalakshmi, M. Priya and S.-C. Kim, Recent advances in catalyst-enhanced luminol chemiluminescence system and its environmental and chemical applications, *J. Environ. Chem. Eng.*, 2023, **11**, 109853.
6 C. Zhang, H. Qi and M. Zhang, Homogeneous electrogenerated chemiluminescence immunoassay for the determination of digoxin employing $Ru(bpy)_2(dcbpy)$ NHS and carrier protein, *Luminescence*, 2007, **22**, 53–59.
7 A. L. Rose and T. D. Waite, Chemiluminescence of luminol in the presence of iron(II) and oxygen: oxidation mechanism and implications for its analytical use, *Anal. Chem.*, 2001, **73**, 5909–5920.
8 W. Gao, C. Wang, K. Muzyka, S. A. Kitte, J. Li, W. Zhang and G. Xu, Artemisinin-luminol chemiluminescence for forensic bloodstain detection using a smart phone as a detector, *Anal. Chem.*, 2017, **89**, 6160–6165.
9 T. Quickenden, C. Ennis and J. Creamer, The forensic use of luminol chemiluminescence to detect traces of blood inside motor vehicles, *Luminescence*, 2004, **19**, 271–277.
10 M. Liang and X. Yan, Nanozymes: from new concepts, mechanisms, and standards to applications, *Acc. Chem. Res.*, 2019, **52**, 2190–2200.
11 Y. Ai, Z. N. Hu, X. Liang, H. b. Sun, H. Xin and Q. Liang, Recent advances in nanozymes: from matters to bioapplications, *Adv. Funct. Mater.*, 2022, **32**, 2110432.
12 M. H. Mahana, M. Sherazee, P. Das, S. R. Ahmed, S. Srinivasan and A. R. Rajabzadeh, Strong nanozymatic activity of silicene quantum dots: Enhanced sensitivity for the selective detection of H_2O_2 and dopamine in complex media, *Microchem. J.*, 2025, **212**, 113278.
13 Z. Sun, Q. Liu, X. Wang, J. Wu, X. Hu, M. Liu, X. Zhang, Y. Wei, Z. Liu and H. Liu, Bioorthogonal catalytic nanozyme-mediated lysosomal membrane leakage for targeted drug delivery, *Theranostics*, 2022, **12**, 1132.
14 S. R. Ahmed, M. Sherazee, P. Das, J. Dondapati, S. Srinivasan and A. R. Rajabzadeh, Borophene quantum dots with enhanced nanozymatic activity for the detection of H_2O_2 and cardiac biomarkers, *ACS Appl. Nano Mater.*, 2023, **6**, 19939–19946.
15 J. Shan, J. Che, C. Song and Y. Zhao, Emerging antibacterial nanozymes for wound healing, *Smart Med.*, 2023, **2**, e20220025.
16 W. Tang, X. Li, M. Lyu and Q. Huang, Cancer cell membrane biomimetic mesoporous nanozyme system with efficient ROS generation for antitumor chemoresistance, *Oxid. Med. Cell. Longevity*, 2022, **2022**, 5089857.
17 X. Li, L. Wang, D. Du, L. Ni, J. Pan and X. Niu, Emerging applications of nanozymes in environmental analysis: Opportunities and trends, *TrAC, Trends Anal. Chem.*, 2019, **120**, 115653.
18 W. C. Hu, M. R. Younis, Y. Zhou, C. Wang and X. H. Xia, In situ fabrication of ultrasmall gold nanoparticles/2D MOFs hybrid as nanozyme for antibacterial therapy, *Small*, 2020, **16**, 2000553.
19 C. Liu, W. Fan, W. X. Cheng, Y. Gu, Y. Chen, W. Zhou, X. F. Yu, M. Chen, M. Zhu and K. Fan, Red emissive carbon dot superoxide dismutase nanozyme for bioimaging and ameliorating acute lung injury, *Adv. Funct. Mater.*, 2023, **33**, 2213856.
20 B. Das, J. L. Franco, N. Logan, P. Balasubramanian, M. I. Kim and C. Cao, Nanozymes in point-of-care diagnosis: an emerging futuristic approach for biosensing, *Nano-Micro Lett.*, 2021, **13**, 193.
21 A. Giussani, P. Farahani, D. Martínez-Muñoz, M. Lundberg, R. Lindh and D. Roca-Sanjuán, Molecular basis of the chemiluminescence mechanism of luminol, *Chem.–Eur. J.*, 2019, **25**, 5202–5213.
22 B. Radwan, H. Liu and D. Chaudhury, The role of dopamine in mood disorders and the associated changes in circadian rhythms and sleep-wake cycle, *Brain Res.*, 2019, **1713**, 42–51.
23 G. Ayano, Dopamine: receptors, functions, synthesis, pathways, locations and mental disorders: review of literatures, *J. Ment. Disord. Treat.*, 2016, **2**, 2.
24 H. Y. Yue, H. J. Zhang, S. Huang, X. X. Lu, X. Gao, S. S. Song, Z. Wang, W. Q. Wang and E. H. Guan, Highly sensitive and selective dopamine biosensor using Au nanoparticles-ZnO nanocone arrays/graphene foam electrode, *Mater. Sci. Eng., C*, 2020, **108**, 110490.
25 S. R. Ahmed, J. Kim, T. Suzuki, J. Lee and E. Y. Park, Enhanced catalytic activity of gold nanoparticle-carbon nanotube hybrids for influenza virus detection, *Biosens. Bioelectron.*, 2016, **85**, 503–508.
26 S. R. Ahmed, K. Takemeura, T.-C. Li, N. Kitamoto, T. Tanaka, T. Suzuki and E. Y. Park, Size-controlled preparation of peroxidase-like graphene-gold nanoparticle hybrids for the visible detection of norovirus-like particles, *Biosens. Bioelectron.*, 2017, **87**, 558–565.
27 J. R. Stone and S. Yang, Hydrogen peroxide: a signaling messenger, *Antioxid. Redox Signaling*, 2006, **8**, 243–270.
28 K. Dhara and D. R. Mahapatra, Recent advances in electrochemical nonenzymatic hydrogen peroxide sensors based on nanomaterials: a review, *J. Mater. Sci.*, 2019, **54**, 12319–12357.
29 J. E. Giaretta, H. Duan, F. Oveissi, S. Farajikhah, F. Dehghani and S. Naficy, Flexible sensors for hydrogen peroxide detection: A critical review, *ACS Appl. Mater. Interfaces*, 2022, **14**, 20491–20505.
30 B. E. Watt, A. T. Proudfoot and J. A. Vale, Hydrogen peroxide poisoning, *Toxicol. Rev.*, 2004, **23**, 51–57.
31 S. Liao, M. Zhao, J. Luo, K. Luo, J. Wu, R. Liu, S. Wang, P. Jia, Y. Bai and X. Zheng, The interaction mechanism between alkaloids and pepsin based on lum-AuNPs in the

chemiluminescence analysis, *RSC Adv.*, 2019, **9**, 25569–25575.
32 X. Zhang, H. Zhang, S. Xu and Y. Sun, A highly sensitive LED-induced chemiluminescence platform for aptasensing of platelet-derived growth factor, *Analyst*, 2014, **139**, 133–137.
33 S. Al-Sodies, A. M. Asiri, M. Alam, K. A. Alamry, M. A. Hussein and M. M. Rahman, Sensitive Cr^{3+} sensor based on novel poly(luminol-co-1,8-diaminonaphthalene)/CeO_2/MWCNTs nanocomposites, *RSC Adv.*, 2024, **14**, 5797–5811.
34 V. S. Ajay Piriya, P. Joseph, S. C. G. Kiruba Daniel, S. Lakshmanan, T. Kinoshita and S. Muthusamy, Colorimetric sensors for rapid detection of various analytes, *Mater. Sci. Eng., C*, 2017, **78**, 1231–1245.
35 M. Sherazee, P. K. Marvi, P. Das, S. R. Ahmed, S. Srinivasan and A. R. Rajabzadeh, Silicene's intriguing nanozymatic activity: Improved colorimetric and electrochemically supported colorimetric biosensing, *Microchem. J.*, 2024, **201**, 110616.
36 C. Tan, N. Gao, Y. Deng, Y. Zhang, M. Sui, J. Deng and S. Zhou, Degradation of antipyrine by UV, UV/H_2O_2 and UV/PS, *J. Hazard. Mater.*, 2013, **260**, 1008–1016.
37 R. D. Bach and H. B. Schlegel, Bond dissociation energy of peroxides revisited, *J. Phys. Chem. A*, 2020, **124**, 4742–4751.
38 J. Yi, C. Bahrini, C. Schoemaecker, C. Fittschen and W. Choi, Photocatalytic decomposition of H_2O_2 on different TiO_2 surfaces along with the concurrent generation of HO_2 radicals monitored using cavity ring down spectroscopy, *J. Phys. Chem. C*, 2012, **116**, 10090–10097.
39 G. Lee, C. Kim, D. Kim, C. Hong, T. Kim, M. Lee and K. Lee, Multibranched Au–Ag–Pt nanoparticle as a nanozyme for the colorimetric assay of hydrogen peroxide and glucose, *ACS Omega*, 2022, **7**, 40973–40982.
40 J. Guo, Y. Liu, Z. Mu, S. Wu, J. Wang, Y. Yang, M. Zhao and Y. Wang, Label-free fluorescence detection of hydrogen peroxide and glucose based on the Ni-MOF nanozyme–induced self-ligand emission, *Microchim. Acta*, 2022, **189**, 219.
41 X. Ji, Q. Lu, X. Sun, L. Zhao, Y. Zhang, J. Yao, X. Zhang and H. Zhao, Dual-active Au@PNIPAm nanozymes for glucose detection and intracellular H_2O_2 modulation, *Langmuir*, 2022, **38**, 8077–8086.
42 R. Tian, J. Sun, Y. Qi, B. Zhang, S. Guo and M. Zhao, Influence of VO_2 nanoparticle morphology on the colorimetric assay of H_2O_2 and glucose, *Nanomaterials*, 2017, **7**, 347.
43 J. He, D. He, L. Yang, G.-L. Wu, J. Tian, Y. Liu and W. Wang, Preparation of urchin-like Pd-Pt-Ir nanozymes and their application for the detection of ascorbic acid and hydrogen peroxide, *Mater. Lett.*, 2022, **314**, 131851.
44 R. Baron, M. Zayats and I. Willner, Dopamine-, L-DOPA-, adrenaline-, and noradrenaline-induced growth of Au nanoparticles: assays for the detection of neurotransmitters and of tyrosinase activity, *Anal. Chem.*, 2005, **77**, 1566–1571.
45 M. Marieeswaran and P. Panneerselvam, Transition metal coordination frameworks as artificial nanozymes for dopamine detection via peroxidase-like activity, *Mater. Adv.*, 2021, **2**, 7024–7035.
46 M. Noroozifar, M. Khorasani-Motlagh, R. Akbari and M. B. Parizi, Simultaneous and sensitive determination of a quaternary mixture of AA, DA, UA and Trp using a modified GCE by iron ion-doped natrolite zeolite-multiwall carbon nanotube, *Biosens. Bioelectron.*, 2011, **28**, 56–63.
47 M. Sherazee, S. R. Ahmed, P. Das, S. Srinivasan and A. R. Rajabzadeh, Electrochemically enhanced peroxidase-like activity of nanohybrids for rapid and sensitive detection of H_2O_2 and Dopamine, *Colloids Surf., A*, 2023, **679**, 132576.
48 S. R. Ahmed, A. G. Cardoso, H. V. Cobas, P. Das, A. Chen, S. Srinivasan and A. R. Rajabzadeh, Graphdiyne quantum dots for H_2O_2 and dopamine detection, *ACS Appl. Nano Mater.*, 2023, **6**, 8434–8443.
49 W. Liu, R. Tian, Z. Peng, S. Yang, X. xiao Liu, Y. Yang, W. Zhang and L. Liu, Nonlinear responses of the V_{max} and K_m of hydrolytic and polyphenol oxidative enzymes to nitrogen enrichment, *Soil Biol. Biochem.*, 2020, **141**, 107656.
50 Y.-M. Wang, J.-W. Liu, J.-H. Jiang and W. Zhong, Cobalt oxyhydroxide nanoflakes with intrinsic peroxidase catalytic activity and their application to serum glucose detection, *Anal. Bioanal. Chem.*, 2017, **409**, 4225–4232.
51 A. Asati, S. Santra, C. Kaittanis, S. Nath and J. M. Perez, Oxidase-like activity of polymer-coated cerium oxide nanoparticles, *Angew. Chem.*, 2009, **121**, 2344–2348.
52 A. Dalui, B. Pradhan, U. Thupakula, A. H. Khan, G. S. Kumar, T. Ghosh, B. Satpati and S. Acharya, Insight into the mechanism revealing the peroxidase mimetic catalytic activity of quaternary CuZnFeS nanocrystals: colorimetric biosensing of hydrogen peroxide and glucose, *Nanoscale*, 2015, **7**, 9062–9074.
53 S. Keerthana, A. Rajapriya, C. Viswanathan and N. Ponpandian, Enzyme like-colorimetric sensing of H_2O_2 based on intrinsic peroxidase mimic activity of WS_2 nanosheets anchored reduced graphene oxide, *J. Alloys Compd.*, 2021, **889**, 161669.
54 S. Cai, Q. Han, C. Qi, Z. Lian, X. Jia, R. Yang and C. Wang, $Pt_{74}Ag_{26}$ nanoparticle-decorated ultrathin MoS_2 nanosheets as novel peroxidase mimics for highly selective colorimetric detection of H_2O_2 and glucose, *Nanoscale*, 2016, **8**, 3685–3693.
55 L. Lin, X. Song, Y. Chen, M. Rong, T. Zhao, Y. Wang, Y. Jiang and X. Chen, Intrinsic peroxidase-like catalytic activity of nitrogen-doped graphene quantum dots and their application in the colorimetric detection of H_2O_2 and glucose, *Anal. Chim. Acta*, 2015, **869**, 89–95.
56 N. Wang, J. Sun, L. Chen, H. Fan and S. Ai, A $Cu_2(OH)_3Cl$-CeO_2 nanocomposite with peroxidase-like activity, and its application to the determination of hydrogen peroxide, glucose and cholesterol, *Microchim. Acta*, 2015, **182**, 1733–1738.
57 S. Singh, K. Mitra, R. Singh, A. Kumari, S. K. S. Gupta, N. Misra, P. Maiti and B. Ray, Colorimetric detection of

hydrogen peroxide and glucose using brominated graphene, *Anal. Methods*, 2017, **9**, 6675–6681.

58 Y. Liu, C. Wang, N. Cai, S. Long and F. Yu, Negatively charged gold nanoparticles as an intrinsic peroxidase mimic and their applications in the oxidation of dopamine, *J. Mater. Sci.*, 2014, **49**, 7143–7150.

59 X. Jiang, C. Sun, Y. Guo, G. Nie and L. Xu, Peroxidase-like activity of apoferritin paired gold clusters for glucose detection, *Biosens. Bioelectron.*, 2015, **64**, 165–170.

60 P. Bilalis, E. Karagouni and D. K. Toubanaki, Peroxidase-like activity of Fe_3O_4 nanoparticles and Fe_3O_4-graphene oxide nanohybrids: Effect of the amino- and carboxyl-surface modifications on H_2O_2 sensing, *Appl. Organomet. Chem.*, 2022, **36**, e6803.

61 X.-Q. Zhang, S.-W. Gong, Y. Zhang, T. Yang, C.-Y. Wang and N. Gu, Prussian blue modified iron oxide magnetic nanoparticles and their high peroxidase-like activity, *J. Mater. Chem.*, 2010, **20**, 5110–5116.

62 M. Ma, J. Xie, Y. Zhang, Z. Chen and N. Gu, Fe_3O_4@Pt nanoparticles with enhanced peroxidase-like catalytic activity, *Mater. Lett.*, 2013, **105**, 36–39.

63 R. Ezzatfar, G. Dehghan, M. Amini and A. Khataee, Synthesis of Peroxidase-Like V_2O_5 Nanoparticles for Dye Removal from Aqueous Solutions, *Top. Catal.*, 2022, 1–9.

